Letters in Applied NanoBioScience
Open-Access Journal (ISSN: 2284-6808)

Article
Volume 15, Issue 1, 2026, 6
https://doi.org/10.33263/LIANBS151.006

In Silico Analysis of Phytocompounds from *Alpinia officinarum* Targeting Staphyloxanthin Biosynthetic Pathway Proteins in *Staphylococcus aureus*

Narmadha Alagirisamy [1], Hemalatha Srinivasan [1,*]

[1] School of Life Sciences, B. S. Abdur Rahman Crescent Institute of Science and Technology, Chennai, India; narmadhaa_sls_jan21@crescent.education (N.A.); hemalatha.sls@bsauniv.ac.in (H.S.);
* Correspondence: hemalatha.sls@bsauniv.ac.in;

Received: 6.10.2025; Accepted: 10.02.2026; Published: 30.03.2026

Abstract: The increasing prevalence of antibiotic-resistant *Staphylococcus aureus* has necessitated the search for alternative therapeutic strategies targeting bacterial virulence factors. Staphyloxanthin, a golden carotenoid pigment, contributes to *S. aureus* virulence by protecting the bacterium against reactive oxygen species (ROS) and host neutrophil-mediated killing. This study aimed to identify phytocompounds from *Alpinia officinarum* capable of inhibiting key enzymes involved in staphyloxanthin biosynthesis using in silico approaches. Thirty bioactive phytocompounds were screened through molecular docking against three target enzymes—C(30) carotenoid dehydrosqualene synthase (CrtM), staphyloxanthin protein, and 4, 4′-diaponeurosporene aldehyde dehydrogenase (AldH1). Quercetin exhibited the strongest binding affinities of −8.10 kcal/mol (staphyloxanthin), −6.18 kcal/mol (CrtM), and −9.12 kcal/mol (AldH1), forming multiple hydrogen and hydrophobic interactions with active site residues. Molecular dynamics simulation (100 ns) revealed the stability of the quercetin–protein complexes, with average RMSD fluctuations below 2.0 Å and consistent radius of gyration (Rg) and hydrogen bond profiles, confirming structural compactness. Pharmacokinetic and drug-likeness analyses using Lipinski's rule of five and SwissADME indicated favorable ADME properties for most compounds. Overall, quercetin and related phytoconstituents from *A. officinarum* demonstrate strong potential as natural anti-virulence agents targeting the staphyloxanthin biosynthetic pathway in *S. aureus.*

Keywords: molecular dynamic simulation; molecular docking; *Staphylococcus aureus*; staphyloxanthin; *Alpinia officinarum*; phytocompounds.

1. Introduction

The global escalation of antibiotic resistance poses a serious threat to public health, necessitating the discovery of alternative therapeutic strategies to combat drug-resistant pathogens. *Staphylococcus aureus* remains one of the most clinically significant pathogens, responsible for life-threatening infections such as pneumonia, sepsis, and endocarditis, which contribute to considerable morbidity and mortality worldwide [1–3]. The emergence of multidrug-resistant strains, including methicillin-resistant *S. aureus* (MRSA), has rendered many conventional antibiotics ineffective, intensifying the need for innovative approaches that target bacterial virulence rather than viability [4, 5].

One of the key virulence determinants of *S. aureus* is staphyloxanthin, a golden carotenoid pigment that imparts antioxidant protection by neutralizing reactive oxygen species (ROS) produced by host immune cells [6]. This pigment enhances bacterial resistance to

oxidative killing and facilitates immune evasion, thereby promoting persistent infection [7]. Inhibition of the staphyloxanthin biosynthetic pathway represents a promising anti-virulence strategy, as it can attenuate bacterial pathogenicity without exerting strong selective pressure for resistance development.

Alpinia officinarum Hance (lesser galangal), a traditional medicinal plant native to China, is widely recognized for its pharmacological properties, including antimicrobial, antioxidant, and anti-inflammatory activities. Its rhizomes are rich in bioactive flavonoids such as galangin and quercetin, which have demonstrated potent antibacterial and enzyme-inhibitory effects in previous studies [8,9]. Given these properties, *A. officinarum* phytochemicals were hypothesized to interact with and inhibit key enzymes in the staphyloxanthin biosynthetic pathway of *S. aureus*, thereby reducing virulence potential.

Molecular docking is a well-established computational technique used to predict the binding affinity, orientation, and molecular interactions between potential ligands and target proteins, thereby enabling the identification of novel inhibitors at the molecular level [10–14]. Complementarily, molecular dynamics (MD) simulations provide time-dependent insights into the stability, flexibility, and conformational dynamics of protein–ligand complexes, validating docking results and assessing the persistence of interactions under near-physiological conditions [15,16].

Therefore, the present study aimed to evaluate the inhibitory potential of phytocompounds from *A. officinarum* against staphyloxanthin biosynthetic proteins of *S. aureus* using an integrated in silico approach involving molecular docking and molecular dynamics simulations. The best-docked compound, quercetin, was further analyzed for complex stability through MD simulations. Additionally, Lipinski's Rule of Five and SwissADME analyses were employed to assess the pharmacokinetic properties and drug-likeness of the identified phytocompounds

2. Materials and Methods

2.1. Databases and software used.

2.1.1. Databases used: Pubchem, Genbank, Protein Databank.

The chemical structures of the ligands were obtained from PubChem, while information on the genes and sequences was obtained from GenBank. The three-dimensional structures of the target proteins were obtained from the Protein Data Bank.

2.1.2. Software used: Open bable, Autodock 4.2.6, Biovia Discovery studio.

To perform the computational study, various bioinformatics tools, including molecular docking tools, were used. Open Babel was used to perform ligand format conversion. AutoDock 4.2.6 was used to perform molecular docking, which helped predict binding affinity and interactions between ligands and target proteins. BIOVIA Discovery Studio was used to visualize the interactions.

2.2. Ligand preparation.

Thirty bioactive compounds from *Alpinia officinarum* collected from public databases and published research papers were downloaded from https://pubchem.ncbi.nlm.nih. gov in SDF format (Figure 1). OpenBabel (http://openbabel.org/wiki/Main_Page) was used to change

SDF to PDB format, which makes them suitable for docking analysis. This was followed by setting the torsion requirements for proper binding using Autodock 4.2.6 parameters.

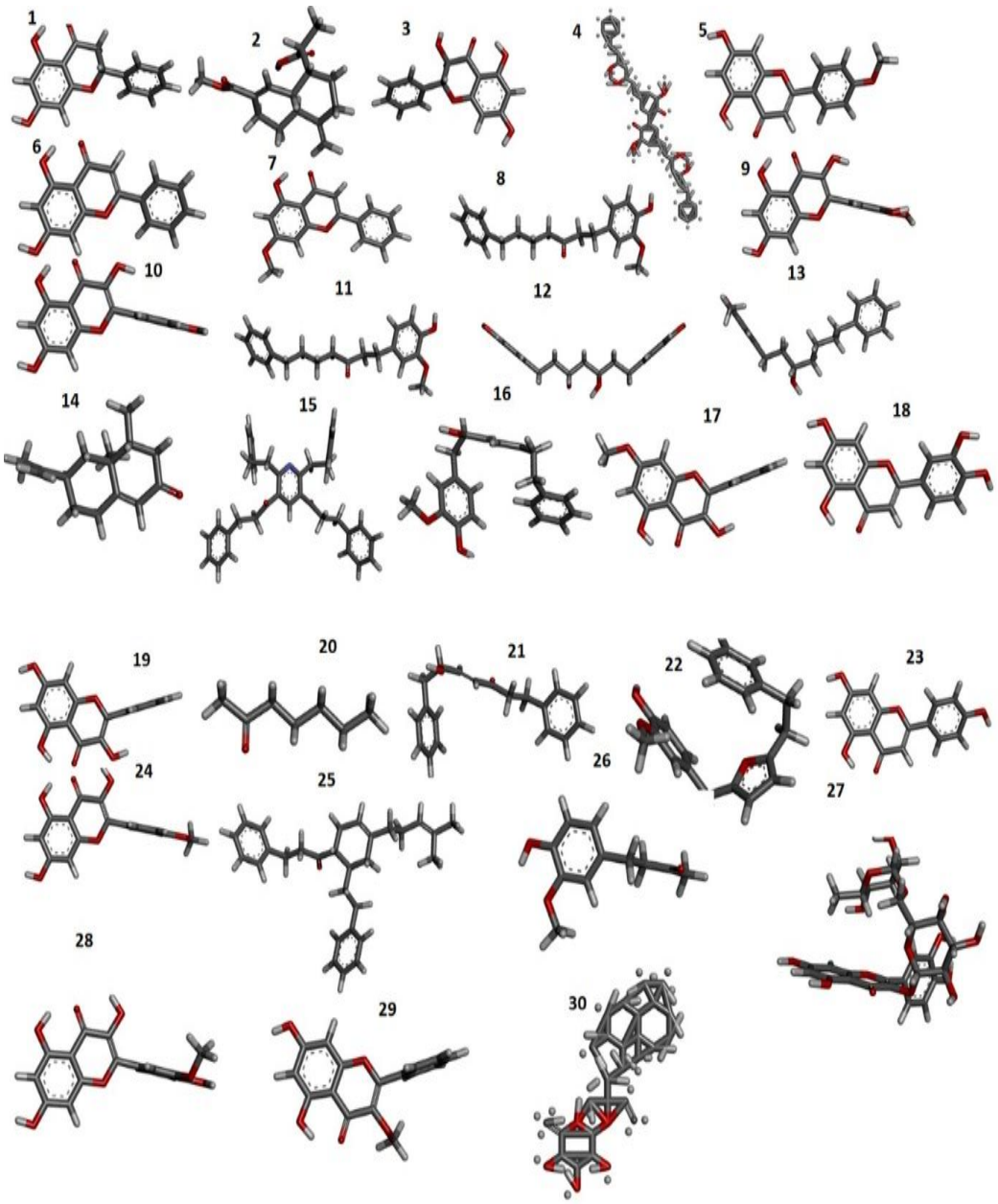

Figure 1. Phytocompounds of *Alpinia officinarum* retrieved from Pubchem**: 1.** Pinocembrine; **2.** Alpiniaterpene A; **3.** Pinobaskin; **4.** Alpinoid A; **5.** Acacetin; **6.** Chrysin; **7.** Tectochrysin; **8.** Yakuchinone; **9.** Quercetin; **10.** Kaempferol; **11.** Hexahydrocurcumin; **12.** Hannokinol; **13.** Oxyphyllacinol; **14.** Nootkatone; **15.** Officinaruminane A; **16.** Alpinoid B; **17.** Izalphin; **18.** Luteolin; **19.** Galangin; **20.** 2 Heptanone; **21.** Alpinoid C; **22.** Alpinoid D; **23.** Apigenin; **24.** Kaemferide; **25.** Officinaruminane B; **26.** Zingerone; **27.** Rutin; **28.** Isorhamnetin; **29.** Galangin 3 methyl ether; **30.** Labdane diterpene**.**

2.3. Protein preparation.

3D structures of C(30) carotenoid dehydrosqualene synthase(CrtM), staphyloxanthin protein and with 4, 4′-diaponeurosporen-aldehyde dehydrogenase protein (aldH1) were downloaded from RCSB protein data bank (http://www.rcsb.org/pdb/home/home.do) with PDB ID 3nri for CrtM, 2lrj for staphyloxanthin protein, 6k10 for aldH1. Autodock 4.2.6 was used for the removal of water molecules and addition of polar hydrogen and Kollman's charges, and these proteins were saved in PDBQT format.

2.4. Molecular docking analysis.

Molecular docking was performed using AutoDock 4.2.6 integrated with MGL Tools 1.5.7, which is widely used for reliable prediction of ligand–protein interactions due to its efficient Lamarckian Genetic Algorithm (LGA) and validated scoring functions [17-19]. The 3D structures of target proteins were obtained from the Protein Data Bank (PDB) and prepared by removing water molecules and adding polar hydrogens and Kollman charges. Ligand structures were energy-minimized using the MMFF94 force field in Chem3D to achieve optimal geometry prior to docking. Docking calculations were conducted using the genetic algorithm search method with a grid box size of 60 × 60 × 60 Å and a grid spacing of 0.5 Å, parameters optimized to encompass the entire active site region of the receptor as reported in previous studies [20, 21]. The grid box was centered on the active-site residues, as determined from the literature and PDB annotations, to ensure accurate ligand placement. The grid box dimensions (60 × 60 × 60 Å) were optimized to fully encompass the active sites of CrtM, aldH1, and the staphyloxanthin protein, ensuring complete ligand accessibility. The Lamarckian Genetic Algorithm (LGA) was selected for its efficiency in exploring conformational space and yielding reproducible docking conformations.

Docking grid parameter files (.gpf) and docking parameter files (.dpf) were generated using AutoDock Tools and executed through AutoGrid and AutoDock modules, respectively. The resulting docking log file (.dlg) was analyzed to obtain the lowest binding energy conformations. The workflow was verified by redocking the co-crystallized ligand to its original binding site, yielding an RMSD of < 2.0 Å, confirming the reliability of the docking protocol. The best-docked receptor–ligand complexes were further analyzed for hydrogen bonding, hydrophobic interactions, binding energy, and inhibition constant (Ki) using BIOVIA Discovery Studio Visualizer 2021.

2.5. Rule of five (RO5).

Lipinski's RO5 was performed to know the drug-likeliness characteristics of the phytocompounds used (http://www.scfbioiitd.res.in/software/drugdesign/lipinski.jsp, Lipinski CA 2004). This is a necessary step in drug discovery that helps to determine whether a certain compound is likely to be orally active. Bioactive compounds with high binding energy were subjected to this analysis.

2.6. SwissADME analysis.

Physicochemical properties such as water solubility, GI absorption, blood-brain barrier permeation, lipophilicity, PGP substrate, Lipinski violation, drug-like nature, and Pharmacokinetic properties were computed by SwissADME (http://www.swissadme.ch/index.php).

2.7. Molecular dynamics simulation.

Molecular dynamics (MD) simulations were performed using the WebGRO server, an online interface based on the GROMACS (GROningen MAchine for Chemical Simulations) package, to evaluate the structural stability and conformational dynamics of the best docked protein–ligand complexes. The GROMOS96 43a1 force field was selected for protein parameterization, while ligand topology files were generated using the PRODRG server from

the ligand's minimized structure. The protein–ligand complex (PDB format) was uploaded and converted into the GROMACS-compatible format for subsequent simulation steps.

The complex was solvated in a triclinic box using the Simple Point Charge (SPC) water model, maintaining a 1.0 nm distance between the solute and box edge. The system was neutralized by adding counter ions (Na^+ or Cl^-) to balance the net charge. Energy minimization was carried out using the steepest descent algorithm for 50, 000 steps or until the maximum force was less than 1000 kJ/mol/nm, ensuring the removal of steric clashes and unfavorable contacts.

Following minimization, equilibration was performed in two sequential phases: NVT (constant Number, Volume, Temperature) ensemble for 100 ps to stabilize system temperature at 300 K, regulated using the Berendsen thermostat. NPT (constant Number, Pressure, Temperature) ensemble for 100 ps to equilibrate system pressure at 1 bar, maintained by the Parrinello–Rahman barostat.

After equilibration, a 100 ns production MD simulation was executed with an integration time step of 2 fs, saving trajectory coordinates every 10 ps. The Periodic Boundary Conditions (PBC) were applied in all directions to mimic an infinite system.

Output files including trajectory (.xtc), energy (.edr), log (.log), and final structure (.gro) files were analyzed to evaluate system stability and conformational changes. The root mean square deviation (RMSD), root mean square fluctuation (RMSF), radius of gyration (Rg), solvent-accessible surface area (SASA), and hydrogen bond (H-bond) profiles were calculated to assess structural compactness, flexibility, and interaction stability. The overall energy and temperature profiles confirmed system equilibration and simulation reliability.

3. Results and Discussion

3.1. Swiss ADME of phytocompounds from Alpinia offficinarum.

Here, in this study, physicochemical and pharmacokinetic properties of ligands from *Alpinia officinarum* were computed using SwissADME, and most of the phytocompounds showed high GI absorption, good blood-brain barrier permeation, and lipophilicity, with no PGP substrate except officinaruminane A, officinaruminane B, alpinoid A, and rutin. All the other compounds showed 0 Lipinski violations with good drug-like nature, and all the compounds had good inhibitory activity (Additional experimental data can be found in Table S1 in the Supplementary Materials).

3.2. Lipinski's RO5 of phytocompounds from Alpinia officinarum.

Lipinski's RO5 showed drug-likeliness characteristics of thirty phytocompounds, and all thirty phytocompounds used in this study did not violate Lipinski's RO5. Additional experimental data can be found in Table S2 in the Supplementary Material.

Pharmacokinetic properties were predicted using Lipinski's RO5 and Swiss ADME, which states that orally active drugs must have fewer than two violations. Swiss ADME enables the estimation of essential ADME characteristics, which provide greater support for pharmacokinetic optimization and the evaluation of small molecules [22].

3.3. Molecular docking.

Autodock 4.2.6 and MGL tools used in this study showed the preferred orientation of thirty phytocompounds from *Alpinia officinarum* with the receptor staphyloxanthin protein,

and its active binding site was predicted. Among thirty phytocompounds examined, quercetin showed better interaction with the protein with high binding energy.

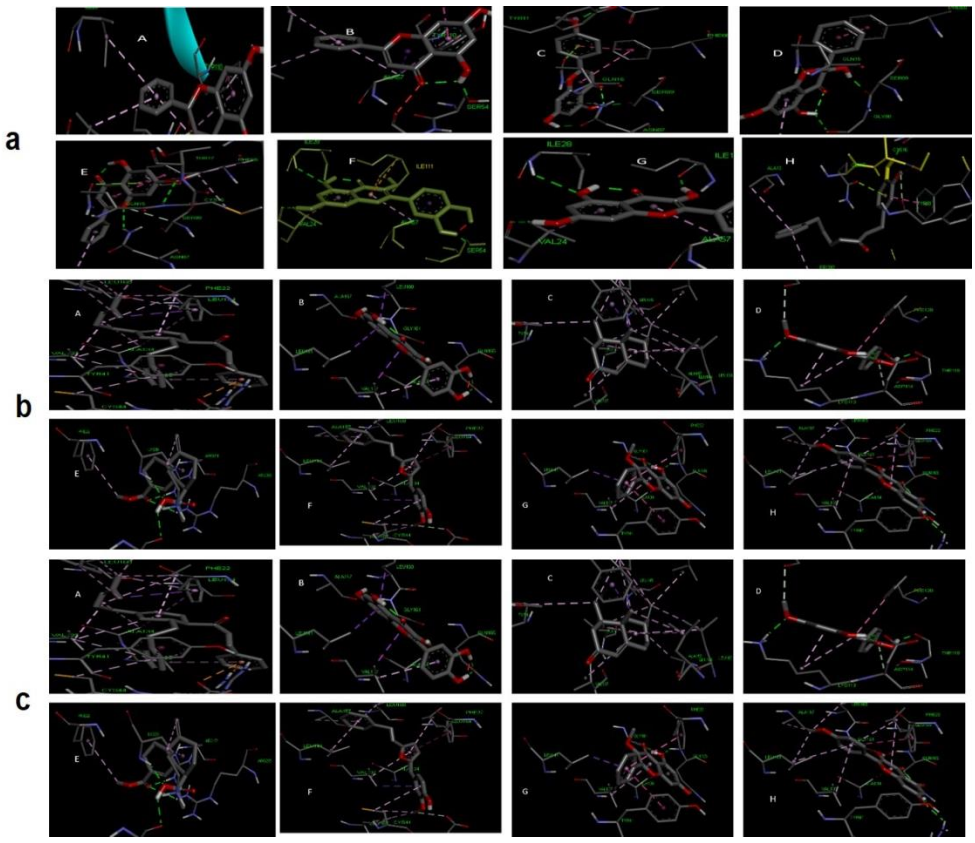

Figure 2. Molecular interactions of *Alpinia officinarum* phytocompounds with key enzymes involved in staphyloxanthin biosynthesis in *Staphylococcus aureus*. **(a)** Interaction of staphyloxanthin protein with ligands from *A. officinarum*: (A) Pinocembrine, (B) Pinobanksin, (C) Acacetin, (D) Chrysin, (E) Tectochrysin, (F) Quercetin, (G) Kaempferol, (H) Hexahydrocurcumin; **(b)** Interaction of C_{30}-carotenoid dehydrosqualene synthase (CrtM) with ligands from *A. officinarum*: (A) Officinaruminane B, (B) Quercetin, (C) Nootkatone, (D) Izalpinin, (E) Alpiniaterpene A, (F) Alpinoid D, (G) Galangin-3-methyl ether, (H) Kaemferide; **(c)** Interaction of 4, 4′-Diaponeurosporene-aldehyde dehydrogenase (AldH) with ligands from *A. officinarum*: (A) Acacetin, (B) Alpinoid D, (C) Apigenin, (D) Chrysin, (E) Kaemferide, (F) Kaempferol, (G) Nootkatone, (H) Quercetin.

3.3.1. The interaction of phytocompounds from *Alpinia officinarum* with Staphyloxanthin biosynthesis protein, CrtM, and aldH1 protein.

The staphyloxanthin biosynthesis protein is essential for completing the Staphyloxanthin biosynthetic pathway; inhibition of this protein using phytocompounds blocks the Staphyloxanthin pathway. Thirty phytocompounds from *Alpinia officinarum* were used in this study, which showed stronger binding to the staphyloxanthin protein. Quercetin showed the highest binding energy of -8.1 kcal/mol, with 3 hydrogen bonds, and bound to residues HIS112, ILE28, ILE111, TYR110, SER54, ALA54, GLY56, LYS55, VAL24, and GLU274. Izalpinin showed the highest binding energy of -5.7 kcal/mol with 1 hydrogen bond and bound with TYR88, SER89, PHE66, GLN 75, GLY90, ASN87, PRO92, as shown in Additional experimental data can be found in Table S3 in the Supplementary Materials, best-docked ligand and protein complex (Figure 2a). Quercetin showed good molecular interactions with the active site.

CrtM is the first enzyme that catalyzes the synthesis of dehydrosqualene. Inhibiting CrtM interferes with the staphyloxanthin pathway. All thirty phytocompounds showed good binding energy with CrtM protein, officinaruminane B showed highest binding energy of -8.66

kcal/mol with 1 hydrogen bond and ligand binding residue side in GLY151, LEU164, GLN185, ASN158, VAL133, VAL137, PHE22, PHE26, ASP48, TYR41, LYS44, ARG45 while alpiniaterpene A showed highest binding energy of -7.83 kcal/mol with 3 hydrogen bonds and ligand binding residue side in LYS273, SER21, SER19, LYS20, TYR248, ARG265, LYS17, HIS18 (Additional experimental data can be found in Table S4 in the Supplementary Materials), best docked complex were shown in Figure 2b, active site of officinaruminane B showed different interactions with the receptors.

4, 4′-diaponeurosporen-aldehyde dehydrogenase protein aldH1 is a newly identified enzyme involved in the biosynthesis of staphyloxanthin. Thirty phytocompounds showed good binding energy with 4, 4′-diaponeurosporen-aldehyde dehydrogenase protein in the range of -3.85 to -11.47 kcal/mol. Quercetin showed 5 hydrogen bonds and ligand binding residues in LEU120, GLN119, ILE66, LEU397, THR62, ALA398, ALA61, MET395, LEU394, VAL245, THR243, ASN115, SER244, TYR116 with high binding energy. Kaempferide showed the highest binding energy of -8.45kcal/mol with 3 hydrogen bond and ligand binding residue side in ILE66, ALA398, LEU397, MET895, ALA61, LEU394, THR62, GLN119, LEU120, TYR116, THR167, ASN116, SER244, THR243 Additional experimental data can be found in Table S5 in the Supplementary Materials, best docked protein-ligand complex were shown in the Figure 2c, active site of quercetin showed weak attractive force, unfavourable donor-donor bond with the receptors. Molecular docking analysis of *Alpinia officinarum* phytocompounds revealed significant binding affinities toward the key enzymes involved in the staphyloxanthin biosynthetic pathway of *Staphylococcus aureus*, indicating their potential as anti-virulence agents. Among the tested compounds, quercetin, galangin, and kaempferol exhibited the strongest binding energies and the most stable hydrogen-bonding interactions with the catalytic residues of CrtM and other virulence-associated proteins. These findings suggest that these flavonoids can effectively occupy the enzyme active sites, potentially blocking the conversion of farnesyl diphosphate to staphyloxanthin intermediates, a mechanism consistent with previously reported natural inhibitors of the pathway [23-27], molecular docking is used to study the active site of ligand and receptor, docking forms a stable complex of protein and ligand, ligand complex was formed by hydrogen bond, hydrophobic bond and Vander Waal's force Comparatively, quercetin demonstrated superior binding affinity (−9.12 kcal/mol) and a higher number of hydrogen and hydrophobic interactions compared to galangin and kaempferol, indicating a stronger stabilization within the binding pocket. This observation aligns with prior docking studies on *S. aureus* virulence proteins, in which quercetin derivatives showed high inhibitory activity due to their polyhydroxylated aromatic structures, which favor π–π stacking and hydrogen bonding with key residues [28-33].

Phytocompounds of *Alpinia officinarum* showed antimicrobial activity by inhibiting staphyloxanthin pathway proteins, including staphyloxanthin protein, CrtM, and aldH1 protein. The antioxidant property of staphyloxanthin, a virulent carotenoid pigment, was inhibited by phytocompounds.

3.4. Molecular dynamics simulation.

Molecular dynamics simulations of the Staphyloxanthin protein, CrtM, and aldH1 were performed with the ligand quercetin to study changes in the protein and the ligand complex, and these results were compared with those from simulations of the protein alone.

The conformational changes and backbone dynamics of the staphyloxanthin–quercetin complex and the staphyloxanthin protein were studied by analyzing RMSD. RMSD plots of

the staphyloxanthin protein showed stability at 0.5 nm, whereas the staphyloxanthin protein and its complex showed stability at 0.4 nm and remained stable until 100 ns. Docking of the protein with the ligand showed a difference in stability, as shown in Figure 3a. RMSD value of CrtM with quercetin stabilizes at 0.15 nm and was stable till 100 ns, whereas RMSD of ligand stabilizes at 1.3 nm and showed stability till 100 ns, as shown in Figure 3b. RMSD value of aldH1 complexed with quercetin stabilizes at 0.3nm and is stable till 100 ns. The addition of the ligand increased the stability of the complex, as shown in Figure 3c.

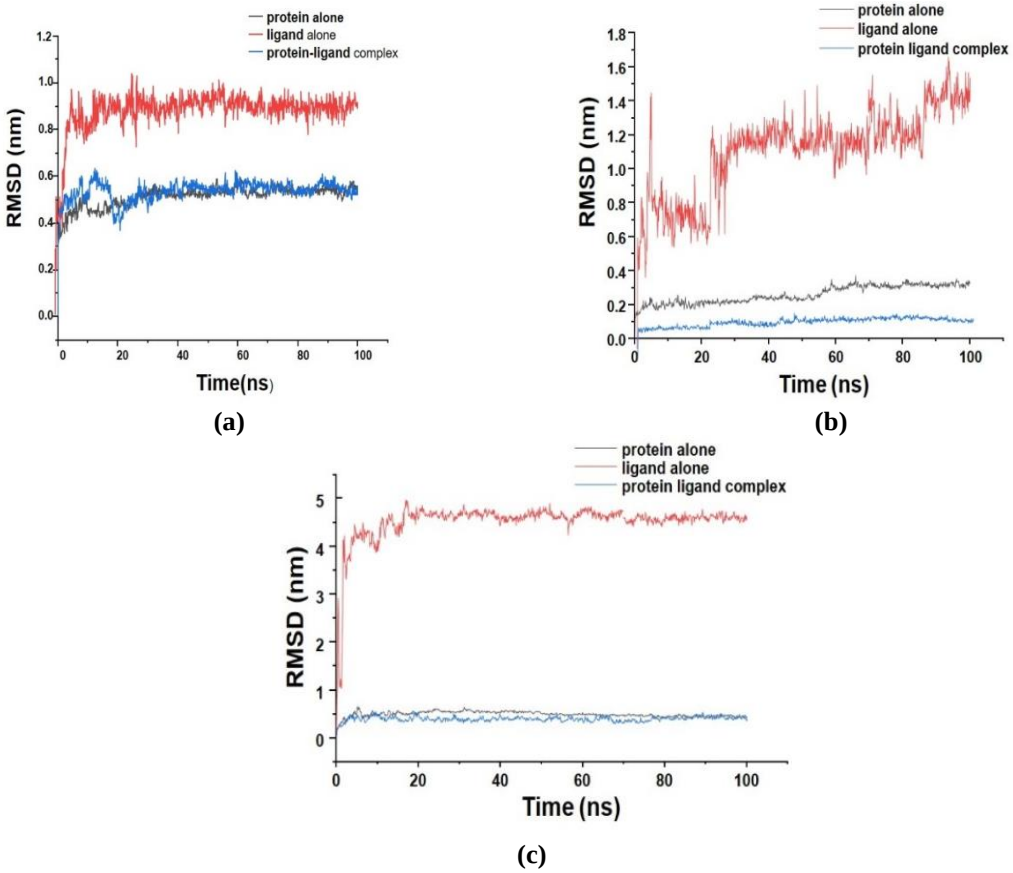

Figure 3. Root mean square deviation plot: **(a)** Staphyloxanthin protein alone, ligand (quercetin) alone, staphyloxanthin protein with quercetin complex; **(b)** CrtM protein alone, ligand (quercetin) alone, CrtM protein with quercetin complex; **(c)** aldH1 protein alone, ligand (quercetin) alone, aldH1 protein with quercetin complex.

Root mean square fluctuation showed fluctuations in the C-terminal atoms. The RMSF profile of the staphyloxanthin protein with quercetin complex was compared with the RMSF values of the protein alone. The RMSF data showed a stable complex formed by the staphyloxanthin protein, with a fluctuation at 0.9 nm and a peak at the forty-fifth residue, as shown in Figure 4a. RMSF fluctuation was stable in the CrtM protein alone, while the CrtM protein with quercetin complex showed fluctuation at 0.7 nm, and fluctuation was reduced after the addition of ligand, as shown in Figure 4b. RMSF of the aldH1 protein alone showed fluctuation at 0.4 nm, and the addition of ligands increased the fluctuation. AldH1 protein with quercetin complex showed fluctuation at 0.3 nm, and the complex showed high fluctuation at 450th residue, as shown in Figure 4c.

The radius of gyration of staphyloxanthin protein with quercetin complex showed high stability. The binding of the ligand decreased the Rg value, which shows high stability and compactness, as shown in Figure 5a. Rg of CrtM protein with quercetin complex showed high stability and compactness of the protein, as shown in Figure 5b. Rg of aldH1 protein

with quercetin complex showed high stability, and it showed compactness of the protein during protein ligand complex formation, as shown in Figure 5c.

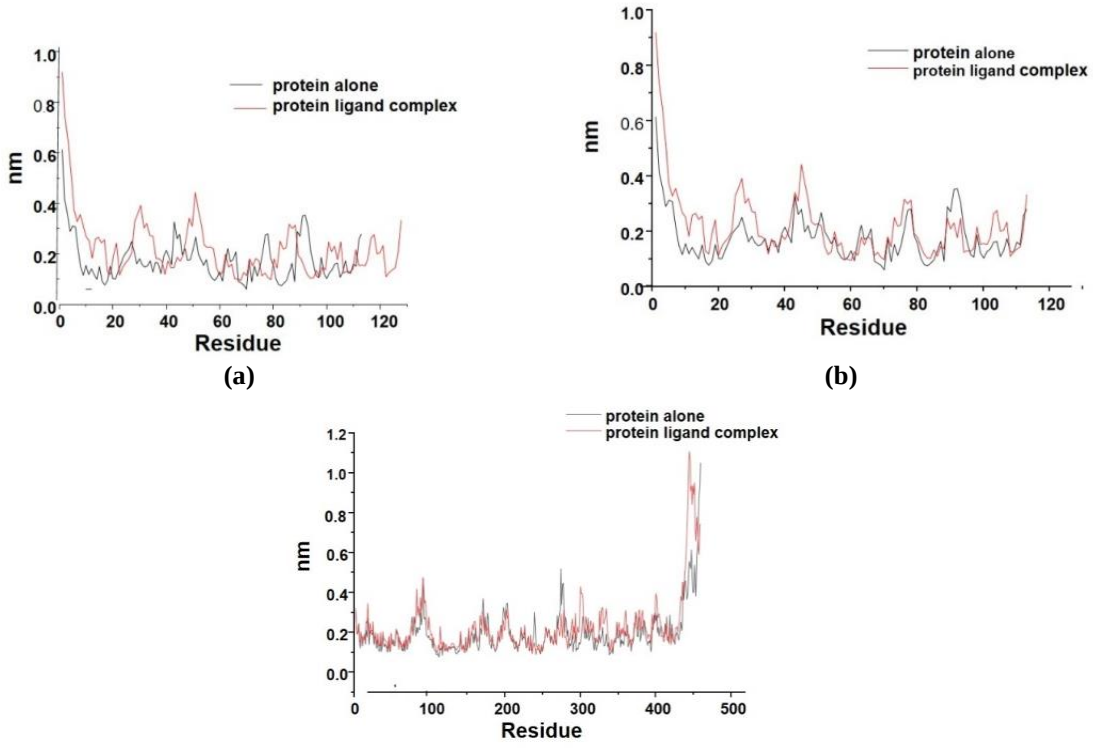

Figure 4. Root mean square fluctuation plot: **(a)** Staphyloxanthin protein alone and staphyloxanthin protein with quercetin; **(b)** CrtM protein alone and CrtM protein with quercetin; **(c)** aldH1 protein alone and aldH1with quercetin.

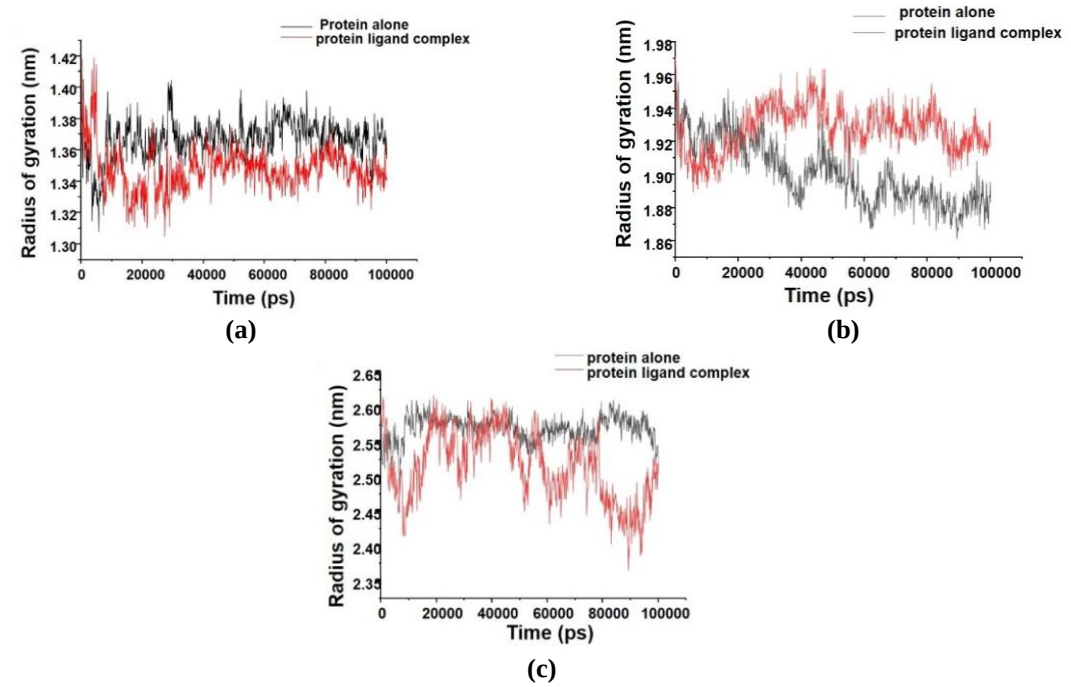

Figure 5. Radius of gyration: **(a) S**taphyloxanthin protein alone and **s**taphyloxanthin with quercetin complex; **(b)** CrtM protein alone and CrtM protein with quercetin complex; **(c)** aldH protein alone and aldH protein with quercetin complex.

SASA of staphyloxanthin protein decreases with increased compactness, leading to differences in SASA-predicted changes in protein structure. SASA of staphyloxanthin protein and quercetin complex showed higher compactness than protein alone, as shown in Figure 6a.

SASA of CrtM protein is reduced at 135 nm^2 with an increase in compactness, which is a difference in SASA predicted changes in the structure of a protein. SASA plot of CrtM protein with quercetin complex is more stable than the protein alone, as shown in Figure 6b. The SASA plot of the aldH1 protein with quercetin shows greater stability than the protein alone, with increased compactness and predicted changes in the structure of the protein, as shown in Figure 6c.

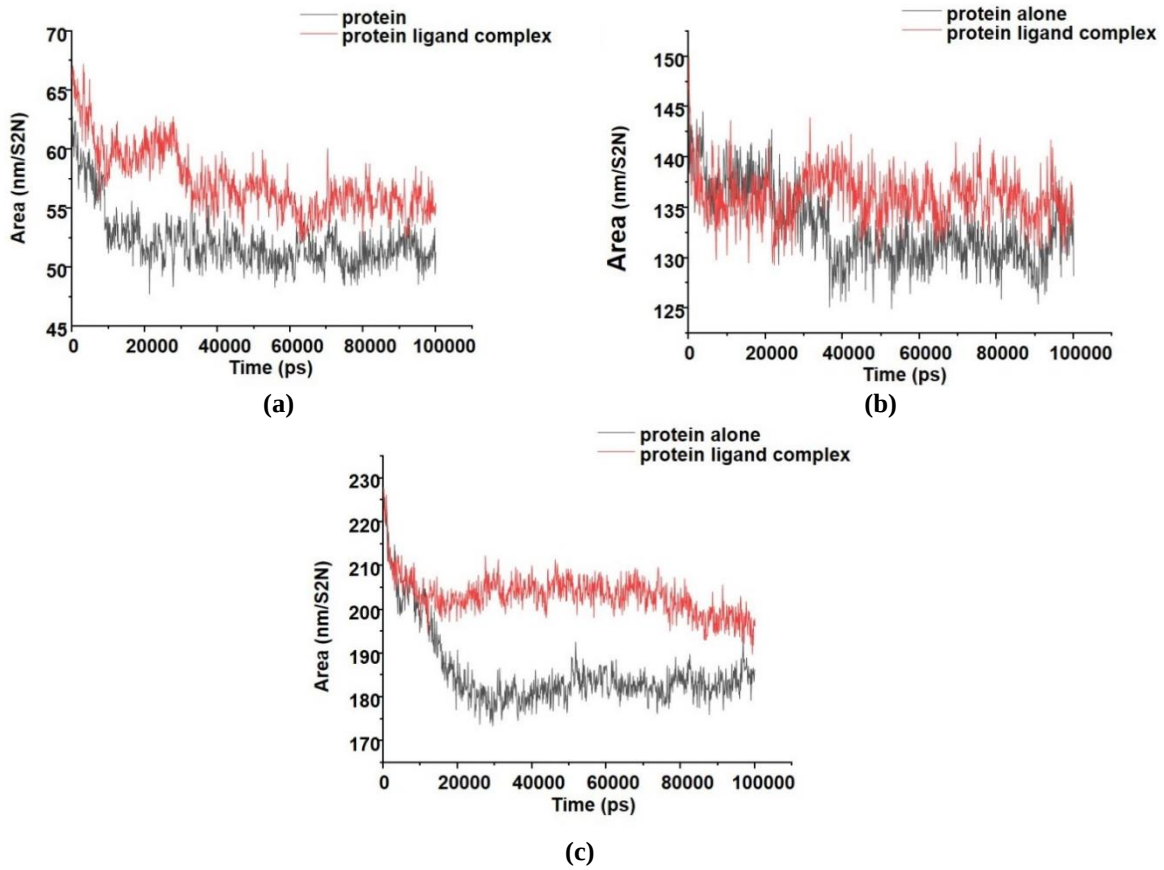

Figure 6. Solvent accessible surface area: **(a)** Staphyloxanthin protein alone and staphyloxanthin protein with quercetin; **(b)** CrtM protein alone and CrtM protein with quercetin; **(c)** aldH1 protein alone and aldH1 protein with quercetin.

A hydrogen bond regulates protein-ligand binding affinity; it also promotes the stability of protein ligand complex and staphyloxanthin protein, while the quercetin ligand complex showed a higher number of bonds than protein alone, as shown in Figure 7a. CrtM protein complexed with quercetin showed a higher number of hydrogen bonds than protein alone, as shown in Figure 7b. The aldH1 protein complexed with quercetin showed a higher number of hydrogen bonds than the protein alone, as shown in Figure 7c.

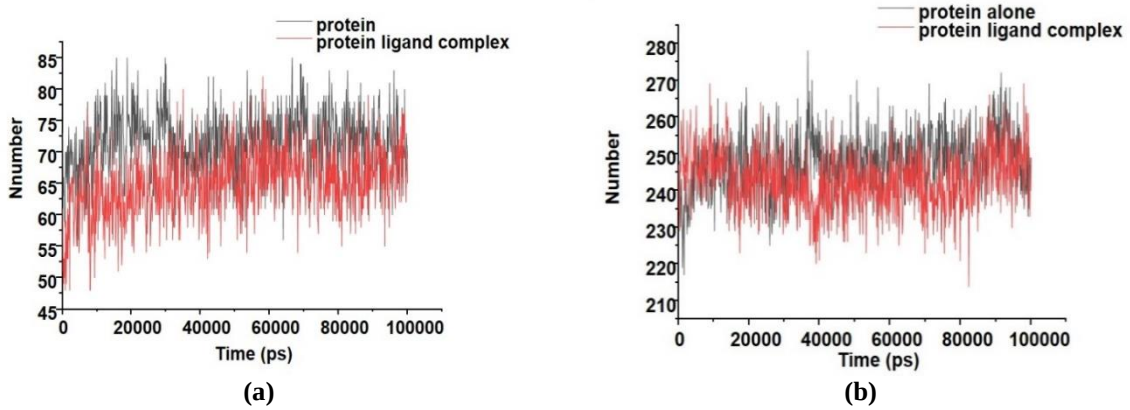

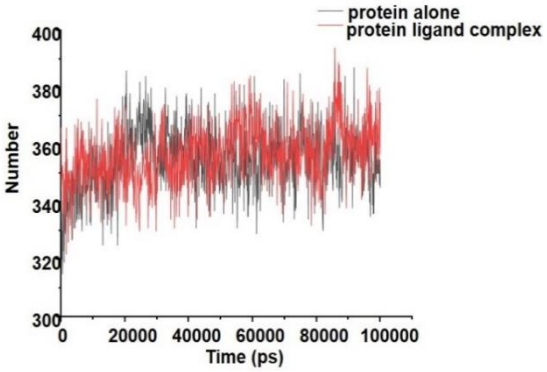

(c)

Figure 7. Prediction of Hydrogen bond: **(a)** Staphyloxanthin protein alone and staphyloxanthin protein with quercetin complex; **(b)** CrtM protein alone and CrtM protein with quercetin complex; **(c)** aldH1 protein alone and aldH1 protein with quercetin complex.

In this study, molecular dynamics simulation was performed using the best-docked complex and RMSD, RMSF, Rg, and SASA. A hydrogen bond was predicted using the WebGro server, which showed the protein's flexibility and stability, as well as changes in its structure due to ligand binding.

These findings are consistent with earlier reports that flavonoids, particularly quercetin derivatives, exhibit high inhibitory potential against *S. aureus* virulence proteins due to their flexible aromatic scaffolds and strong hydrogen-donating ability [23–27]. Molecular dynamics (MD) simulations further substantiated the docking results, showing that the quercetin–CrtM complex maintained stable conformations throughout the 100 ns trajectory, with minimal RMSD fluctuations (<2.0 Å) and a stable radius of gyration (~18.6 Å). The RMSF analysis revealed limited atomic flexibility at the binding site, indicating reduced conformational mobility upon ligand binding. Furthermore, quercetin complexes showed lower solvent-accessible surface area (SASA) values compared to the other flavonoids, confirming a more compact and solvent-shielded protein–ligand conformation.

Overall, these comparative analyses reveal that quercetin forms the most stable and energetically favorable complexes among all *A. officinarum* phytochemicals tested. Its ability to maintain persistent hydrogen bonding and compact binding conformations throughout the simulation indicates strong inhibitory potential against staphyloxanthin biosynthetic enzymes. These computational results align with experimental findings from prior literature, supporting the biological plausibility of *A. officinarum* flavonoids as promising candidates for anti-virulence therapy targeting *S. aureus* pathogenicity [28–33].

All thirty phytocompounds from *Alpinia officinarum* used in this study do not violate Lipinski's RO5 and showed inhibitory activity against the staphyloxanthin pathway proteins. 4, 4′-diaponeurosporen-aldehyde dehydrogenase protein, which was identified recently as the new target gene involved in the staphyloxanthin synthesis pathway, was used in this study. The MDS showed the compactness and solubility of the complex, which was compared with the protein simulation. Changes in the structure of the protein after ligand binding were observed in this study. Phytocompounds from *Alpinia officinarium* showed good interaction and inhibited staphyloxanthin pathway proteins. The results suggested that phytocompounds from *A. officinarum* can be used as drug candidates for the inhibition of staphyloxanthin production, which can reduce the growth and virulence of *Staphylococcus aureus* [33-37].

MD simulation of protein-ligand complex was performed using a webgro server, which showed the flexibility of residues, binding energy, salt bridge, hydrogen bond interaction in the

binding region, and structural variation during unfolding, beyond docking. Molecular dynamics (MD) simulation confirmed the structural stability of the protein–ligand complexes. The RMSD plots of the top complexes reached equilibrium within 20 ns and remained stable throughout the 100 ns simulation, indicating conformational steadiness of the bound state. Low RMSF values (<1.5 Å) at the active site residues reflected minimal flexibility, confirming the rigidity induced by ligand binding. Concurrently, a decrease in solvent-accessible surface area (SASA) and a consistent radius of gyration (Rg) indicated a more compact protein conformation, suggesting enhanced structural integrity upon ligand interaction. These parameters collectively validate the persistence of the docked pose throughout the simulation period.

The observed inhibitory potential has strong biological plausibility. Inhibition of staphyloxanthin biosynthesis compromises *S. aureus* antioxidant defense mechanisms, rendering the pathogen more susceptible to host immune clearance. Therefore, targeting this pathway offers a feasible anti-virulence strategy that minimizes selective pressure for antibiotic resistance. The pharmacokinetic predictions from SwissADME further revealed that these compounds obey Lipinski's rule, suggesting favorable absorption and bioavailability characteristics necessary for therapeutic applicability.

Overall, integrating docking and MD analyses provides a coherent model supporting the inhibitory role of *A. officinarum* phytocompounds against *S. aureus* virulence. Future studies involving enzymatic inhibition assays and in vivo validation are essential to confirm their efficacy and safety profiles [38-41].

4. Conclusions

This study provides a computational insight into the inhibitory potential of *Alpinia officinarum* phytocompounds against key proteins involved in the staphyloxanthin biosynthetic pathway of *Staphylococcus aureus*. Molecular docking and dynamics simulations suggest that these compounds form stable and favorable interactions with target proteins, indicating their promise as scaffolds for further drug development.

However, as the findings are derived solely from in silico analyses, experimental validation through in vitro and in vivo studies is essential to confirm their biological activity and pharmacokinetic behavior. Future research should explore additional virulence-related targets, perform structure–activity relationship (SAR) studies, and optimize formulation strategies to enhance bioavailability and therapeutic efficacy.

Overall, this work contributes to the early-stage identification of natural compounds with potential anti-virulence properties and underscores the value of computational approaches in guiding antimicrobial drug discovery efforts against antibiotic-resistant *S. aureus*.

Author Contributions

Conceptualization, H.S.; methodology, H.S. and N.A.; validation, H.S. and N.A.; formal analysis, N.A.; investigation, H.S.; data curation, N.A.; writing—original draft preparation, N.A.; writing—review and editing, H.S.; visualization, N.A.; supervision, H.S.; project administration, H.S. All authors have read and agreed to the published version of the manuscript.

Institutional Review Board Statement

Not applicable.

Informed Consent Statement

Not applicable.

Data Availability Statement

Data will be available on request.

Funding

This research received no external funding.

Acknowledgments

The authors are thankful to B.S. Abdur Rahman Institute of Science and Technology, Chennai, for providing research facilities in the School of Life Sciences.

Conflicts of Interest

The authors declare that there is no conflict of interest.

Abbreviations

Abbreviation	Definition
ROS	Reactive Oxygen Species
CrtM	C(30) Carotenoid Dehydrosqualene Synthase
aldH1	4, 4′-diaponeurosporen-aldehyde Dehydrogenase Protein
MDS	Molecular Dynamic Simulation
RMSD	Root Mean Square Deviation
RMSF	Root Mean Square Fluctuation
SASA	Solvent Accessible Surface Area
RG	Radius of Gyration
H bond	Hydrogen Bond

References

1. Touati, A.; Ibrahim, N.A.; Idres, T. Disarming *Staphylococcus aureus*: Review of Strategies Combating This Resilient Pathogen by Targeting Its Virulence. *Pathogens* **2025**, *14*, 386, https://doi.org/10.3390/pathogens14040386.
2. Singh, SK.; Bhattacharjee, M.; Unni, B.; Kashyap, RS.; Malik, A.; Akhtar, S.; Fatima, S. In silico testing to identify compounds that inhibit ClfA and ClfB binding to the host for the formulation of future drugs against Staphylococcus aureus colonization and infection. *Front Cell Infect Microbiol*. **2024**, *14*, 1422500. https://doi.org/10.3389/fcimb.2024.1422500.
3. Morris, S.D.; Kumar, V.A.; Biswas, R.; Mohan**,** C.G. Identification of a *Staphylococcus aureus* amidase catalytic domain inhibitor to prevent biofilm formation by sequential virtual screening, molecular dynamics simulation and biological evaluation. *Int. J. Biol. Macromol.* **2024**, *254*, 127842. https://doi.org/10.1016/j.ijbiomac.2023.127842
4. Rehman, Z.U. Assessing the Inhibitory Potential of Natural Compounds for Targeting the CrtM Proteins in Methicillin-Resistant *Staphylococcus aureus* through Machine Learning-based QSAR Modeling and Structural Dynamics Analysis. *Curr. Med. Chem.* **2025**, *32*, 9344–9366, https://doi.org/10.2174/0109298673340184250120065924.

5. Varghese, A.; Liu, J.; Patterson, T.A.; Hong, H. Integrating Molecular Dynamics, Molecular Docking, and Machine Learning for Predicting SARS-CoV-2 Papain-like Protease Binders. *Molecules* **2025**, *30*, 2985, https://doi.org/10.3390/molecules30142985.
6. Dong, J.; Hao, X.G. Pharmacophore screening, molecular docking, and MD simulations for identification of VEGFR-2 and c-Met potential dual inhibitors. *Front. Pharmacol.* **2025**, *16*, 1534707, https://doi.org/10.3389/fphar.2025.1534707.
7. Kumar, N.; Gond, C.; Singh, J.D.; Datta, A. Molecular docking, pharmacological profiling, and MD simulations of glycolytic inhibitors targeting novel SARS CoV-2 main protease and spike protein. *In Silico Pharmacol.* **2025**, *13*, 44, https://doi.org/10.1007/s40203-025-00336-2.
8. Kashyap, M.; Gupta, S.; Bansal, Y.; Bansal, G. 2D-QSAR driven design, molecular docking, molecular dynamics simulation and MM/GBSA studies on quinazoline derivatives for development of VEGFR-2 inhibitors. *Discov. Chem.* **2025**, *2*, 111, https://doi.org/10.1007/s44371-025-00173-4.
9. Lei, X.; Wang, J.; Zuo, K.; Xia, T.; Zhang, J.; Xu, X.; Liu, Q.; Li, X. *Alpinia officinarum* Hance: a comprehensive review of traditional uses, phytochemistry, pharmacokinetic and pharmacology. *Front. Pharmacol.* **2024**, *15*, 1414635, https://doi.org/10.3389/fphar.2024.1414635.
10. Zagórska, J.; Pietrzak, K.; Kukula-Koch, W.; Czop, M.; Wojtysiak, K.; Koch, W. Influence of Thermal Treatment on the Composition of Alpinia officinarum Rhizome. *Int J Mol Sci*. **2024**, *7*, 3625, https://doi.org/10.3390/ijms25073625.
11. Sadeghian, Z.; Bayat, M.; Gheidari, D. Synthesis, molecular docking, pharmacological evaluation, MD simulation, and DFT calculations of quinazolin-12-one derivatives as PDK1 inhibitors. *Nanoscale Adv.* **2025**, *7*, 5760-5783, https://doi.org/10.1039/D5NA00182J.
12. Gómez Borrego, J.; Torrent Burgas, M. Evaluating ligand docking methods for drugging protein–protein interfaces: insights from AlphaFold2 and molecular dynamics refinement. *J. Cheminform.* **2025**, *17*, 144, https://doi.org/10.1186/s13321-025-01067-4.
13. Singha, J.; Dutta, N.; Saikia, J.P. A novel volatile staphyloxanthin biosynthesis inhibitor against *Staphylococcus aureus. Microb. Pathog.* **2025**, *203*, 107489, https://doi.org/10.1016/j.micpath.2025.107489.
14. Younes, K.M.; Abouzied, A.S.; Alafnan, A.; Huwaimel, B.; Khojali, W.M.A.; Alzahrani, R.M. Investigating the bispecific lead compounds against methicillin-resistant *Staphylococcus aureus* SarA and CrtM using machine learning and molecular dynamics approach. *J. Biomol. Struct. Dyn.* **2025**, *43*, 3348-3365, https://doi.org/10.1080/07391102.2023.2297012.
15. Chauhan, A.; Sharma, P.; Gupta, R.; Sharma, S.; Singh, A.; Singh, M.; Singh, R.; Singh, S.; Kumar, A. Unlocking the Therapeutic Potential of Phytocompounds from Essential Oils of Melaleuca alternifolia and Rosmarinus officinalis Targeting Bacterial Penicillin-Binding Proteins by Computational and Experimental Validation. *Discov. Chem*. **2025**, *2*, 28, https://doi.org/10.1007/s44371-025-00096-0.
16. Deshmukh, H. S.; Patil, S. V.; Yadav, S.; Kumar, M.; Sharma, A.; Singh, S.; Kumar, R.; Kumar, A. An Insightful Review on Molecular Docking Techniques and Their Applications in Drug Discovery. *South Asian Res J Pharm Sci*. **2025**, *4*, 1–10, https:/doi.org/10.36346/sarjps.2025.v07i01.005.
17. Jilla, T. The Role of Molecular Docking in Drug Discovery: Current Approaches and Innovations. *Int. J. Zool. Environ. Life Sci.* **2025**, *2*, 16–20, https://doi.org/10.70604/ijzels.v2i2.55.
18. Kawuma, S.; Bamutura, D.S.; Nura, I.; Ashiraf, D.Z.; Bazira, J. Virtual Toxicity Screening and Molecular Docking of Natural Compounds to Discover New Antibiotics for Methicillin-Resistant *Staphylococcus aureus. Medinformatics* **2025**, *2*, 318–326, https://doi.org/10.47852/bonviewMEDIN52026042.
19. Nivatya, H.K.; Singh, A.; Kumar, N.; Sonam; Sharma, L.; Singh, V.; Mishra, R.; Gaur, N.; Mishra, A.K. Assessing molecular docking tools: understanding drug discovery and design. *Future J. Pharm. Sci.* **2025**, *11*, 111, https://doi.org/10.1186/s43094-025-00862-y.
20. Rastogi, V.; Yadav, R. Targeting Antibiotic Resistance in *Staphylococcus aureus***:** Screening and Docking Study of Phytochemicals as Potential Inhibitors**.** *J. Prev. Diagn. Treat. Strateg. Med.* **2025**, *2*, 130–142, https://doi.org/10.4103/jpdtsm.jpdtsm_38_25.
21. Xu, J.; Chen, J.; Xia, H.; Gong, Y.; Xiong, F. Integrated Approaches for Discovery of *Staphylococcus aureus* Antimicrobial Agents: Virtual Screening, Molecular Docking, Molecular Dynamics Simulations, and Density Functional Theory. *Chem. Biodivers.* **2025**, *22*, e202403449, https://doi.org/10.1002/cbdv.202403449.
22. Bastos, M.L.; Adido, H.E.; Martins de Brito, A.K.; Chagas, C.K.; Castro, A.L.; Ferreira, G.G.; Nascimento, P.H.; Padilha, W.R.; Sarmento, R.M.; Garcia, V.V.; Marinho, A.M.; Marinho, P.S.; Rocha de Oliveira,

J.A.; Vale, V.V.; Percário, S.; Dolabela, M.F. Eleutherin and Isoeleutherin Activity against *Staphylococcus aureus* and *Escherichia coli* Strain's: Molecular Docking and Antibacterial Evaluation. *Int. J. Mol. Sci.* **2024**, *25*, 12583, https://doi.org/10.3390/ijms252312583.

23. Subramani, N.K.; Venugopal, S. Molecular Docking and Dynamic Simulation Studies of Bioactive Compounds from Traditional Medicinal Compounds Against Exfoliative Toxin B from *Staphylococcus aureus*. *J. Pharmacol. Pharmacother.* **2024**, *15*, 316-326, https://doi.org/10.1177/0976500X241266072.
24. Salamat, A.; Kosar, N.; Mohyuddin, A.; Imran, M.; Zahid, M.N.; Mahmood, T. SAR, Molecular Docking and Molecular Dynamic Simulation of Natural Inhibitors against SARS-CoV-2 Mpro Spike Protein. *Molecules* **2024**, *29*, 1144, https://doi.org/10.3390/molecules29051144.
25. Chao, P.; Zhang, X.; Zhang, L.; Yang, A.; Wang, Y.; Chen, X. Integration of molecular docking and molecular dynamics simulations with subtractive proteomics approach to identify the novel drug targets and their inhibitors in *Streptococcus gallolyticus*. *Sci. Rep.* **2024**, *14*, 14755, https://doi.org/10.1038/s41598-024-64769-z.
26. El-Hddad, S.S.A.; Sobhy, M.H.; El-morsy, A.; Shoman, N.A.; El-Adl, K. Quinazolines and thiazolidine-2,4-dions as SARS-CoV-2 inhibitors: repurposing, *in silico* molecular docking and dynamics simulation. *RSC Adv.* **2024**, *14*, 13237-13250, https://doi.org/10.1039/D4RA02029D.
27. da Rocha, J.A.P.; da Costa, R.A.; da Costa, A.d.S.S.; da Rocha, E.C.M.; Gomes, A.J.B.; Machado, A.K.; Fagan, S.B.; Brasil, D.d.S.B.; Lima e Lima, A.H. Harnessing Brazilian biodiversity database: identification of flavonoids as potential inhibitors of SARS-CoV-2 main protease using computational approaches and all-atom molecular dynamics simulation. *Front. Chem.* **2024**, *12*, 1336001, https://doi.org/10.3389/fchem.2024.1336001.
28. Parveen, D.; Sharma, R.; Singh, P.; Ali, R.; Shaquiquzzaman, M.; Azam, F.; Akhter, M.; Gupta, A.; Kumar, V.; Saifullah, M. K.; Khan, M. A.; Parvez, S. Design, Molecular Docking and MD Simulation of Novel Estradiol-Pyrimidine Analogues as Potential Inhibitors of Mpro and ACE2 for COVID-19. *Chem. Phys. Impact* **2024**, *8*, 100560, https://doi.org/10.1016/j.chphi.2024.100560.
29. Mohanasundaram, S.; Karthikeyan, P.; Sampath, V.; Anbazhagan, M.; Venkatesa Prabhu, S.; Khaled, J. M.; Thiruvengadam, M. Molecular Docking, Dynamics Simulations, ADMET, and DFT Calculations: Combined In Silico Approach to Screen Natural Inhibitors of 3CL and PL Proteases of SARS-CoV-2. *BioMed Research International* **2024**, *2024*, 6647757, https://doi.org/10.1155/2024/664775.
30. Alassaf, N.A.; Hamody, A.S.; Jabir, M.S.; Ghotekar, S.; Swelum, A.A. Molecular docking study and pharmacokinetic insights of rifampicin in pure and capsule dosage forms. *Sci. Rep.* **2025**, *15*, 25174, https://doi.org/10.1038/s41598-025-06720-4.
31. Jafari, S.; Bojarska, J. Molecular Docking Study of Natural Compounds Targeting the β2-Adrenergic Receptor (β2-AR). *Med. Sci. Forum* **2025**, *34*, 3, https://doi.org/10.3390/msf2025034003.
32. Sadeghian, S.; Razmi, R.; Khabnadideh, S.; Khoshneviszadeh, M.; Mardaneh, P.; Talashan, A.; Pirouti, A.; Khebre, F.; Zahmatkesh, Z.; Rezaei, Z. Synthesis, biological evaluation, molecular docking, and MD simulation of novel 2,4-disubstituted quinazoline derivatives as selective butyrylcholinesterase inhibitors and antioxidant agents. *Sci Rep* **2024**, *14*, 15577. https://doi.org/10.1038/s41598-024-66424-z.
33. Chikhale, RV.; Choudhary, R.; Eldesoky, GE.; Kolpe, MS.; Shinde, O.; Hossain, D. Generative AI, molecular docking and molecular dynamics simulations assisted identification of novel transcriptional repressor EthR inhibitors to target Mycobacterium tuberculosis. *Heliyon* **2025**, *11*, e42593, https://doi.org/10.1016/j.heliyon.2025.e42593.
34. Singh, S.; Goyal, A.; Agrawal, N. Molecular Docking and Dynamic Simulation to Identify α7nAChR Binding Affinity of Flavonoids for the Treatment of Alzheimer's Disease. *Chem. Biodivers.* **2023**, *20*, e202300306, https://doi.org/10.1002/cbdv.202300306.
35. Zrinej, J.; Elmchichi, L.; Alaqarbeh, M.; Lakhlifi, T.; Bouachrine, M. Computational approach: 3D-QSAR, molecular docking, ADMET, molecular dynamics simulation investigations, and retrosynthesis of some curcumin analogues as PARP-1 inhibitors targeting colon cancer. *New J. Chem.* **2023**, *47*, 20987-21009, https://doi.org/10.1039/D3NJ03981A.
36. Samanta, P.; Mishra, S.K.; Pomin, V.H.; Doerksen, R.J. Docking and Molecular Dynamics Simulations Clarify Binding Sites for Interactions of Novel Marine Sulfated Glycans with SARS-CoV-2 Spike Glycoprotein. *Molecules* **2023**, *28*, 6413, https://doi.org/10.3390/molecules28176413.
37. Ravikumar, Y.; Koonyosying, P.; Srichairatanakool, S.; Ponpandian, L.N.; Kumaravelu, J.; Srichairatanakool, S. In Silico Molecular Docking and Dynamics Simulation Analysis of Potential Histone

Lysine Methyl Transferase Inhibitors for Managing β-Thalassemia. *Molecules* **2023**, *28*, 7266, https://doi.org/10.3390/molecules28217266.
38. Khademi Dehkordi, M.; Hoveida, L.; Fani, N. Structure-based virtual screening, molecular docking, and molecular dynamics simulation approaches for identification of new potential inhibitors of class a β-lactamase enzymes. *J. Biomol. Struct. Dyn.* **2024**, *42*, 5631-5641, https://doi.org/10.1080/07391102.2023.2227724.
39. Mustafa, G.; Younas, S.; Mahrosh, H.S.; Albeshr, M.F.; Bhat, E.A. Molecular Docking and Simulation-Binding Analysis of Plant Phytochemicals with the Hepatocellular Carcinoma Targets Epidermal Growth Factor Receptor and Caspase-9. *Molecules* **2023**, *28*, 3583, https://doi.org/10.3390/molecules28083583.
40. Mavvaji, M.; Muhammed, M.T.; Akkoc, S. Synthesis, Cytotoxic Activity, Docking and MD Simulation of *N*,*N*-Disubstituted New Benzimidazolium Salts. *ChemistrySelect* **2023**, *8*, e202303053, https://doi.org/10.1002/slct.202303053.
41. McNutt, A.T.; Li, Y.; Meli, R.; Aggarwal, R.; Koes, D.R. GNINA 1.3: the next increment in molecular docking with deep learning. *J. Cheminform.* **2025**, *17*, 28, https://doi.org/10.1186/s13321-025-00973-x.

Publisher's Note & Disclaimer

Supplementary materials

Table S1. Swiss ADME showing pharmacokinetic properties of phytocompounds from *Alpinia officinarium*.

S. no	Phytocompounds	Water solubility	GI absorbtion	BBB permeate	Lipophilicity	PGP substrate	Lipinski violation
1	Pinocembrine	-3.64	High	yes	2.11	No	0 violation
2	Alpiniaterpene A	-3.01	High	yes	4.72	No	0 violation
3	Pinobaskin	-2.95	high	no	1.74	No	0 violation
4	Alpinoid A	-7.42	low	no	5.58	Yes	1 violation
5	Acacetin	-4.14	high	no	2.56	No	0 violation
6	Chrysin	-4.19	high	yes	2.27	No	0 violation
7	Tectochrysin	-4.39	high	yes	2.88	No	0 violation
8	Yakuchinone A	-4.03	high	yes	3.58	No	0 violation
9	Quercetin	-3.16	high	no	1.63	No	0 violation
10	Kaempferol	-3.31	high	no	1.70	No	0 violation
11	Hexahydrocurcumin	-3.53	high	no	3.14	Yes	0 violation
12	Hannokinol	-3.71	high	no	2.35	Yes	0 violation
13	Oxyphyllacinol	-4.36	high	yes	3.65	Yes	0 violation
14	Nootkatone	-3.56	high	yes	2.83	No	0 violation
15	Officinaruminane A	-8.22	low	no	4.73	Yes	2 violation
16	Alpinoid B	-3.61	high	yes	3.08	No	0 violation
17	Izalpinin	-3.66	high	no	2.68	No	0 violation
18	Luteolin	-3.71	high	no	1.86	No	0 violation
19	Galangin	-3.46	high	no	2.08	No	0 violation
20	2-heptanone	-1.53	high	yes	2.09	No	0 violation
21	Alpinoid C	-3.68	high	yes	3.07	No	0 violation
22	Alpinoid D	-4.93	high	yes	3.53	No	0 violation
23	Apigenin	-3.94	high	no	1.89	No	0 violation
24	Kaempferide	-3.51	high	no	2.43	No	0 violation
25	Officinaruminane B	-6.68	low	no	4.77	Yes	1 violation
26	Zingerone	-1.80	high	yes	2.09	No	0 violation
27	Rutin	-3.30	low	NO	0.46	Yes	3 violation
28	Isorhamnetin	-3.36	high	NO	2.35	No	0 violation
29	Galangin 3-methyl ether	-4.37	High	No	2.41	No	0 violation
30	Labdanediterpene	-4.92	High	No	4.31	No	0 Violation

Table S2. Lipinski's RO5 analysis of ligands from *Alpinia officinarium*.

S.no	Phytocompounds	mass	H donor	H acceptor	Lipophilicity	Molar refractivity
1	Pinocembrine	256	2	4	2.804299	68.53
2	Alpiniaterpene	278	1	4	2.798	74.876
3	Pinobaksin	272	3	5	1.775100	69.91985
4	Alpinoid A	682	2	8	8.198865	191.57
5	Acacetin	284	2	5	2.722599	75.7010
6	Tectochrysin	268	1	4	3.016998	74.036
7	Chrysin	254	2	4	2.71399	69.1490
8	Yakuchinone A	312	1	3	4.315498	91.983775
9	Quercetin	302	5	7	2.010900	74.050476
10	Kaemferol	286	4	6	2.305299	72.385
11	Hexahydrocurcumin	312	1	3	4.315498	91.983
12	Hannokinol	316	4	4	2.775099	89.4861
13	Oxyphyllacinol	314	2	3	4.107298	92.983566
14	Nootkatone	218	0	1	3.9044199	67.132
15	Officinaruminane A	551	0	3	8.283004	170.124207
16	Alpinoid B	326	2	4	3.06229	93.279572
17	Izalpinin	284	2	5	2.96266	75.6
18	Luteolin	286	4	6	2.925199	72.478676
19	Galangin	270.000000	3	5	2.599699	70.720879
20	2-heptanone	114	0	1	2.15570	34.822
21	Alpinoid C	280.000	1	2	3.34	83.062767
22	Alpinoid D	308	1	3	4.36799	90.02774
23	Apigenin	270.000	3	5	2.419598	70.813881
24	Kaempferide	300	3	6	2.608299	77.272873
25	Officinaruminane B	400	0	1	7.520103	127.494949
26	Zingerone	194	1	3	1.922400	53.660789
27	Rutin	610	10	16	-1.878800	137.495483

28	Isorhamnetin	316	4	7	2.313900	78.937675
29	Galangin 3-methylether	284	2	5	2.688099	75.101074
30	Labdanediterpene	436	3	5	6.059052	136.099380

Table S3. Interaction of phytocompounds from *Alpinia officinarum* with staphyloxanthin protein.

S.no	Phytocompounds	Binding energy (kcal/mol)	Inhibitory constant (µM)	No of hydrogen bonds	Ligand binding residue side
1	Pinocembrine	-5.4	109.95	1	GLY58, SER54, ALA57, ILE58, TYR110, ILE21, HIS112, ILE111
2	Alpiniaterpene A	-4.20	867.18	2	LYS55, SER74, VAL75, SER77, ASN76
3	Pinobaksin	-5.41	108.7	2	TYR88, PRO92, GLY90, ASN87, SER89, GLN15, PHE88
4	AlpinoidA	-3.46	2.9	0	PHE68, SER89, GLN15, GLY33, TRP32, TYR11, SER30, LEU10
5	Acacetin	-5.32	126.8	4	PRO92, GLY90, ASN87, SER89, GLN15, TYR11, ASN34
6	Chrysin	-5.41	108.39	1	ILE28, HIS112, ILE111, TYR110, ILE58, SER54, GLY56, ALA52, LYS55
7	Tectochrysin	-5.41	107.31	1	TYR88, SER89, PHE66, ASN34, GLN15, AN87, GLY90
8	Yakuchinone A	-4.38	617.96	1	ILE113, HIS112, ILE111, ILE28, GLU27, VAL24, ILE58, GLY56, ALA57, LYS55
9	Quercetin	-8.1	63.87	3	HIS112, ILE28, ILE111, TYR110, SER54, ALA54, GLY56, LYS55, VAL24, GLU274
10	Kaempferol	-5.41	108.61	2	GLU27, ILE26, HIS112, ILE111, TYR110, VAL24, GLY56, ALA57, SER54
11	Hexahydrocurcumin	-5.33	124.15	2	TYR88, SER89, PHE66, ASN34, THR12, PHE98, PRO92, GLY14, ASN37, CYS18
12	Hannokinol	-5.14	170.13	4	HIS112, ILE111, TYR110, GLY56, ALA57, LYS23, VAL24, GLU27, ILE28
13	Oxyphyllacinol	-4.66	381.75	1	GLU27, ILE28, HIS112, ILE112, VAL24, GLY56, ILE58, SER64, LYS56
14	Nootkatone	-5.6	78.56	0	GLU24, ILE113, ILE28, HIS112, ILE111, VAL24, GLY56, ALA57
15	Officinaruminane A	-7.2	651.51	5	GLY25, MET86, TYR19, LYS23, ASP22
16	Alpinoid B	-4.47	333.60	8	GLY56, VAL24, ALA57, LE111, TYR110, HIS112, ILE58, LYS55, LE113, ILE28
17	Izalpinin	-5.7	66.18	1	TYR88, SER89, PHE66, GLN15, GLY90, ASN87, PRO92
18	Luteolin	-5.2	154.32	5	SER96, ARG98, HIS66, GLU63, TYR88
19	Galangin	-5.21	152.48	2	GLY56, VAL24, ALA57, LE111, TYR110, HIS112, ILE58, LYS55, LE113, ILE28
20	2-heptanone	-4.88	262.6	1	TYR88, VAL69, GLY67, LYS16, SER89, THR17, PHE66, GLN15, ASN34, ALA35
21	Alpinoid C	-4.98	222.52	1	ALA57, GLU27, ILE113, LE28, VAL24, LYS23, HIS112, LE111, GLY56, LYS55, TYR71, TYR110
22	Alpinoid D	-4.83	287.83	0	GLU27, LYS55, LYS23, VAL24, GLY56, HIS112, TYR71, ALA57, TYR110
23	Apigenin	-5.22	149.54	2	ILE113, GLU27, HIS112, VAL24, ALA57, TYR110
24	Kaempferide	-5.20	154.52	1	ILE111, TYR110, HIS112, ILE28, ALA57, SER54, GLY56, VAL24, GLU27
25	Officinaruminane B	-4.81	296.97	0	ILE111, HIS112, ILE58, ALA57, GLY56, VAL24, ILE113, ILE28, GLU27, LYS55
26	Zingerone	-4.53	480.09	1	ASN34, TYR88, SER89, GYS18, ALA35, GLN15, THR17, VAL69, PHE65
27	Galangin 3-methyl ether	-5.19	157.95	1	SER54, LYS55, GLY56, ALA57, ILE58, VAL24, GLU27, ILE28, TYR110, ILE111, HIS112
28	Isorhamnetin	-5.17	162.42	3	HIS68, GLU63, GLY64, GLU85, ARG98, TYR88, SER89, ASN137, GLY90, GLY91

S.no	Phytocompounds	Binding energy (kcal/mol)	Inhibitory constant (µM)	No of hydrogen bonds	Ligand binding residue side
29	Labdanediterpene	-7.98	1.42	1	TYR110, ILE11, HIS112, ILE8, ALA57, SER54, GLY56, LYS5, ILE28, VAL24
30	Rutin	-3.28	3.95	1	PHE47, ALA45, THR31, SER30, LEU10, ASN9, GLY8, ASP22, TYR21, GLY26, GLY25, GLU27, ILE28

Table S4. Interaction of phytocompoundsfrom *Alpinia officinarum* with C (30) carotenoid dehydrosqualene synthase.

S.no	Phytocompounds	Binding energy (kcal/mol)	Inhibitory constant (µM)	No of hydrogen bonds	Ligand binding residue side
1	Kaempferide	-6.94	8.18	3	GLY181, LEU184, LEU141, GLY138, ALA134, GLN135, TYR41, PHE22, ARG45
2	Officinaruminane B	-8.66	451.88	1	GLY151, LEU164, GLN185, ASN158, VAL133, VAL137, PHE22, PHE26, ASP48, TYR41, LYS44, ARG45
3	Pinocembrine	-6.72	11.95	3	PHE26, PHE22, LEU145, LEU141, GLY138, GLY161, ALA134, GLN165, LEU160, LEU164
4	Zingerone	-4.23	790.75	0	MET15, ARG45, TYR41, CYS44, VAL37, PHE22, PHE26, VAL137
5	Pinobaksin	-6.71	12.08	0	PHE26, MET15, PHE22, LEU164, GLY161, GLN165, ALA134, VAL137, TYR41, VAL37
6	Chrysin	-6.83	9.92	1	ILE241, PHE26, PHE22, LEU145, LEU141, GLY138, LEU168, LEU164, GLN165, ALA134, ALA157, GLY161
7	AlpinoidA	-5.68	69.03	2	LYS273, VAL268, PHE267, SER21, LYS20, ARG265
8	Tectochrysin	-6.77	10.86	0	GLN165, LEU164, ALA134, VAL133, VAL133, LEU141, PHE22, PHE26, TRY41, VAL37, MET15
9	Acacetin	-6.94	8.12	2	LEU164, LEU160, GLN165, GLY161, VAL133, GLY138, ASP48, VAL137
10	YakuchinoneA	-6.72	11.8	0	ALA134, LEU154, PHE22, GLN135, TYR248, PHE26, LEU145, LEU141, VAL132, GLY38
11	Quercetin	-6.18	29.69	2	LEU160, GLN165, GLY161, ALA157, ALA134, VAL133, GLY138, PHE22, PHE26, VAL137, LEU141
12	Oxyphyllacinol	-6.45	18.68	0	GLN165, LEU164, LEU160, PHE26, TYR41, VAL137, CYS44, ARG45, ALA134
13	Nootkatone	-7.17	5.6	0	LEU160, LEU164, GLY161, GLY138, VAL137, LEU145, LEU141, PHE22, PHE26
14	Kaempferol	-6.36	21.18	2	GLN165, LEU164, AKA134, GLY161, GLY138, ARG45, PHE22, TYR41, LEU141
15	Hexahydrocurcumin	-6.66	13.23	1	PHE233, LEU145, PHE26, LEU141, CYS44, ASP48, VAL133, ALA134, GLN185, GLY136, GLY161, ALA157, LEU160
16	Hannokinol	-6.47	17.99	3	PHE22, TYR248, SER19, TYR41, ILE251, ArG171, VAL266, PHE267, ASP48, ILE21, ARG171, ARG265, ARG45
17	Izalpinin	-7.32	4.28	4	ASP114, PHE117, THR118, MET119, PHE120, GLU125, GLY128, LYS113, THR110
18	Luteolin	-6.33	22.94	3	GLN165, VAL183, PHE22, PHE26, LEU141, GLY138, ALA157, LEU160, GLY181
19	Officinaruminane A	-5.35	119.07	0	ASP228, GLN228, LYS231, PHE233, VAL282, ILE235, HIS148, ASP147, GLN152SER234
20	2-heptanone	-4.19	852.45	1	GLU204, ARG171, THR261, LEU170, ASP172, GLU175, VAL173, GLU264, ARG266
21	AlpiniaterpeneA	-7.83	1.81	3	LYS273, SER21, SER19, LYS20, TYR248, ARG171, ARG265, LYS17, HIS18
22	Alpinoid B	-6.60	14.42	1	ALA134, GLN165, VAL137, GLY138, ASN168, GLY161, ALA157, LEU164, LEU160, TYR248, LEU141, LEU145, PHE22, PHE233, ILE241, LEU145, PHE22
23	Alpinoid C	-6.96	7.92	0	LEU164, LEU160, GLY161, PHE22, PHE26, MET15, TYR41VAL37, GLY138, LEU145, VAL137, LEU141

S.no	Phytocompounds	Binding energy (kcal/mol)	Inhibitory constant (µM)	No of hydrogen bonds	Ligand binding residue side
24	Alpinoid D	-7.20	5.29	0	LEU164, LEU160, PHE26, TYR41, HIS45, ASP48, LY844, ALA134, LEU145, GLY138, VAL137
25	Apigenin	-6.53	16.39	1	ILE241, PHE22, PHE26, LEU164, LEU160, PHE233, LEU145, GLY161, GLN165, ALA157, ALA134, GLY138, LEU141
26	Galangin	-6.58	14.99	2	LEU164, LEU141, GLY161, GLY138, TYR41, ARG45, GLN165, ALA
27	Galangin3methyl ether	-7.10	6.3	1	PHE26, PHE22, LY161, GLN165, ALA134, MET15, TYR41, VAL137, VAL133, VAL137, VAL37, LEU141
28	Rutin	-4.88	263.58	7	PHE22, TYR41, HIS18, VAL137, CYS44, ARG45, ARG265, GEN166, ASN66, ARG171, ASP172, VAL133, TYR129, TYR183, ASP176, ASP114, ARG191, ASN179
29	Labdanediterpene	-10.87	10.68	2	ASN168, TYR248, PHE22, PHE26, LEU141, GLY141, GLY138, LEU160, GLY161, ALA134, LEU164, GLN165, VAL137
30	Isorhamnetin	-6.48	17.79	2	ALA244, PHE26, LEU160, PHE22, LEU164, ASN168, GLN165, GLY138, LEU141, VAL137, ALA134, TYR41, ARG45

Table S5. Interaction of phytocompounds from *Alpinia officinarum* with 4, 4′-diaponeurosporen-aldehyde dehydrogenase aldH1 gene.

S.no	Phytocompounds	Binding energy (kcal/mol)	Inhibitory constant (µM)	No. of hydrogen bonds	Ligand binding residue side
1	2-heptanone	-4.40	592.71	1	Leu120, Tyr415, His416, Leu397, SER244, GLN119, Thr243, VAL245
2	Acacetin	-8.19	1.0	2	Thr243, ASN115, SER244, Tyr118, Leu304, ACA61, Met396, Leu120, Thr187, ILE66, Leu397, ALA396
3	AlpiniaterpeneA	-7.06	6.64	1	Tyr413, His416, Ile86, Leu397, Leu394, Thr62, Tyr116, Leu120, Gln119
4	AlpinoidA	-3.85	1.52	1	Gly413, Gly405, Pro403, Gly406, Gly386, Gly387, Phe385
5	AlpinoidB	-7.32	22.51	1	LEU120, HIS416, ILE66, PHE404, LEU397, ALA398, ALA61, LEU394, TYR116, ASN115, SER244, THR187
6	AlpinoidC	-7.24	4.93	1	LEU120, HIS416, GLN119, LEU397, ILE66, THR62, LEU394, TYR116, THR243, ASN115
7	AlpinoidD	-8.37	738.22	1	THR187, LEU120, PHE404, SER244, ILE66, LEU397, ALA61, TYR116, ASN116
8	Apigenin	-8.08	1.19 µM	3	ASN115, SER244, LEU120, TYR415, TYR116, GLN119, THR62, PHE404, HIS416, ALA61, ILE66, LEU397
9	Chrysin	-8.03	1.29	2	LEU120, TYR415, HIS416, ILE66, LEU397, THR62, TYR116, ASN115, SER244
10	Galangin	-7.76	2.06	2	TYR415, HIS416, PHE404, ILE66, LEU397, LEU394, THR62, TYR116, ASN116, SER144, LEU120
11	Hannokinol	-6.46	18.35	3	LEU120, TYR415, HIS416, GLN119, PHE404, THR62, LEU394, LEU397, TYR116, LEU394, THR238, PHE234
12	Hexahydrocurcumin	-7.26	4.79	1	LEU120, THR187, PHE404, GLN119, LEU397, ALA398, MET395, LEU394, TYR116, SER244, ASN115, THR243
13	Izalpinin	-7.41	3.72	3	MET395, LEU394, SER244, THR62, LEU397, LEU120, GLN119, HIS416, ILE66, ASN116
14	Kaempferide	-8.45	667.1	3	ILE66, ALA398, LEU397, MET895, ALA61, LEU394, THR62, GLN119, LEU120, TYR116, THR167, ASN116, SER244, THR243
15	Kaempferol	-8.44	651.79	3	ASN115, THR243, TYR116, SER244, LEU120, GLN119, THR62, ILE66, LEU397, ALA61, LEU394, MET395, ALA398

S.no	Phytocompounds	Binding energy (kcal/mol)	Inhibitory constant (µM)	No. of hydrogen bonds	Ligand binding residue side
16	Luteolin	-8.21	959.99	3	SER244, TYR116, ASN115, THR243, VAL245, LEU394, ALA61, THR625, LEU397, MET395, ALA61, THR62, LEU397, ALA398, LEU397, ILE66
17	Nootkatone	-8.06	1.24	0	THR243, TYR116, SER244, LEU397, ILE66, GLN119, PHE404, HIS416, LEU120
18	Officinaruminane A	-6.99	7.48	0	THR62, LYS69, ILE66, LEU397, ALA396, MET395, LEU394, TYR60, GLY65, ILE66
19	Officinaruminane B	-7.38	4.03	0	ILE66, GLN119, THR62, TYR116, ALA61, LEU297, ALA393, MET395, LEU394, PHE
20	Oxyphyllacinol	-7.50	3.2	3	THR187, GLU210, LEU120, ASN115, TYR116, THR62, THR62, GLN119, LEU394, LEU397, HIS416, PHE404, LEU84, SER244
21	Pinobaksin	-7.74	2.13	2	LEU120, GLN119, ILE66, LEU397, ALA398, THR62, ALA61, MET395, LEU394, THR243, TYR116
22	Pinocembrine	-8.09	1.17	2	LEU120, TYR415, HIS416, ILE66, PHE404, LEU397, THR62, TYR116, ASN115
23	Quercetin	-9.12	206.56	5	LEU120, GLN119, ILE66, LEU397, THR62, ALA398, ALA61, MET395, LEU394, VAL245, THR243, ASN115, SER244, TYR116
24	Tectochrysin	-7.64	2.52	2	THR243, ASN115, SER244, THR62, GLN119, LEU120, HIS416, LEU397, MET395, LEU394
25	Yakuchinone A	-7.9	1.63	1	LEU120, HIS416, GLN119, LEU397, ALA398, THR62, MET395, LEU394, TYR116, SER244, ASN115, THR187, PHE404
26	Zingerone	-5.84	52.4	1	GLN119, THR62, SER244, TYR116, THR243, ASN115
27	Isorhamnetin	-7.96	1.46	2	LEU120, GLN119, PHE404, ILE66, LEU397, ALA398, MET398, LEU394, ALA61, THR62, ASN115, THR243, TYR116, SER244
28	Galangin3methylether	-7.78	1.99	2	HIS410, ILE66, LEU397, ALA61, LEU394, THR82, VAL245, SER244, THR243, TYR116, ASN115, LEU120, GLN119, TYR415, PHE404
29	Labdanediterpene	-11.47	3.93	1	TYR415, PHE404, ILE66, LEU397, ALA61, THR62, VAL245, THR243, SER244, TYR116, ASN115, GLN119, LEU120, THR187
30	Rutin	-4.77	319.58	6	SER384, PHE385, GLY386, GLY387, GLY388, GLY406, GLY405, GLY413, HIS396, LEU402, PRO403, PHE404, ARG414